The Astrophysical Journal, 783:11 (13pp), 2014 March 1 doi:10.1088/0004-637X/783/1/11

A SMALL-SCALE ERUPTION LEADING TO A BLOWOUT MACROSPICULE JET IN AN ON-DISK CORONAL HOLE

Mitzi Adams, Alphonse C. Sterling, Ronald L. Moore, and G. Allen Gary[1]
Space Science Office, ZP13, NASA Marshall Space Flight Center, Huntsville, AL 35812, USA;
mitzi.adams@nasa.gov, alphonse.sterling@nasa.gov, ron.moore@nasa.gov, gag0002@uah.edu
Received 2013 March 22; accepted 2013 December 19; published 2014 February 7

ABSTRACT

We examine the three-dimensional magnetic structure and dynamics of a solar EUV-macrospicule jet that occurred on 2011 February 27 in an on-disk coronal hole. The observations are from the *Solar Dynamics Observatory* (*SDO*) Atmospheric Imaging Assembly (AIA) and the *SDO* Helioseismic and Magnetic Imager (HMI). The observations reveal that in this event, closed-field-carrying cool absorbing plasma, as in an erupting mini-filament, erupted and opened, forming a blowout jet. Contrary to some jet models, there was no substantial recently emerged, closed, bipolar-magnetic field in the base of the jet. Instead, over several hours, flux convergence and cancellation at the polarity inversion line inside an evolved arcade in the base apparently destabilized the entire arcade, including its cool-plasma-carrying core field, to undergo a blowout eruption in the manner of many standard-sized, arcade-blowout eruptions that produce a flare and coronal mass ejection. Internal reconnection made bright "flare" loops over the polarity inversion line inside the blowing-out arcade field, and external reconnection of the blowing-out arcade field with an ambient open field made longer and dimmer EUV loops on the outside of the blowing-out arcade. That the loops made by the external reconnection were much larger than the loops made by the internal reconnection makes this event a new variety of blowout jet, a variety not recognized in previous observations and models of blowout jets.

Key words: Sun: chromosphere – Sun: filaments, prominences – Sun: magnetic fields – Sun: transition region – Sun: UV radiation

Online-only material: animations

1. INTRODUCTION

A variety of small-scale chromospheric and transition-region jet-like eruptive features exists between the size scale of solar spicules (lengths ∼5000 km; e.g., Beckers 1972) and surges (∼50,000 km; e.g., Roy 1973). Many of these are most easily identifiable near the limb, and frequently in polar regions, which suggests a coronal hole connection. Bohlin et al. (1975), observing in EUV, referred to a class of such features as macrospicules, and Moore et al. (1977) found chromospheric counterparts to these in Hα. On-disk identification of the limb features has been a challenging endeavor, with some authors differentiating between two or more classes of such jets, calling some "macrospicules" and others erupting "minifilaments" or other designations, based on the characteristics of the on-disk features (Labonte 1979; Wang et al. 2000; Innes et al. 2009).

It is strongly suspected that the driving mechanism of at least some macrospicules and other jets is magnetic (e.g., Blake & Sturrock 1985). From studies in soft X-rays, there is evidence that X-ray bright points and X-ray jet features in coronal holes are created when magnetic flux emerges into the photosphere and chromosphere, expands into the corona, and reconnects with a nearby or overlying open magnetic field (Shibata et al. 1992). This provokes the question of whether the same mechanism could explain other jet-like ejective phenomena, even on the scale of spicules (e.g., Moore et al. 1977); spicules are of a size scale smaller than that of macrospicules (few $\times 10^4$ km) and much smaller than that of X-ray jets ($\sim 10^5$ km; discussed in Sterling 2000). Moreover, at least some X-ray jets have counterparts in EUV (e.g., Moore et al. 2010), and also in cool chromospheric lines (Sterling et al. 2010b; Kamio et al. 2010; Huang et al. 2012); in those cases the same mechanism results in emissions across each of these wavelength regimes. Zhang et al. (2000) present two suggestions for macrospicule formation. One is similar to the emerging-flux X-ray jet mechanism, with an emerging bipole interacting with an open field. Their second suggestion is based on cancellation between oppositely directed network fields directly below (at least in their schematic) where the macrospicule forms.

With the excellent temporal and spatial resolution of the telescopes of the *Solar Dynamics Observatory* (*SDO*) Atmospheric Imaging Array (AIA), we have the opportunity to examine on-disk macrospicule-scale jet development in ways not possible in earlier periods. We can also compare the jet's evolution in EUV images with magnetic field structure using the *SDO* Helioseismic and Magnetic Imager (HMI) magnetograph.

Here we report on the detailed evolution of a jet that occurred in a coronal hole located on-disk. Although jet features ranging from spicules (Beckers 1972) to X-ray jets (Cirtain et al. 2007) are prominent in polar coronal hole regions, an advantage of observing them not far from disk center is that the behavior of the magnetic field can be much more easily examined with line-of-sight magnetograms, compared to events near or at the solar limb. Therefore, this event allows us to check whether this jet is caused by emerging flux, or might perhaps erupt via a different mechanism. Work by Nisticò et al. (2010) argues from a statistical standpoint that on-disk coronal hole jets are similar to polar coronal-hole jets. Thus our observations here may apply to other jets as well, but just how general they are will have to await examination of more events.

[1] Center for Space Plasma and Aeronomic Research, The University of Alabama in Huntsville, Huntsville, AL 35805, USA.

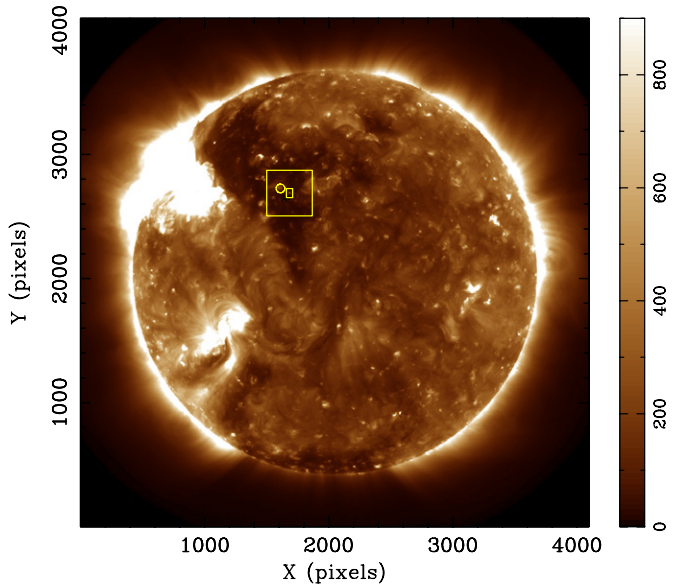

Figure 1. Full-disk AIA 193 Å image. Illustrated are the regions-of-interest within the on-disk coronal hole. The large rectangle is intended to draw the eye to the regions of interest, where the small rectangle surrounds the location of the jet. The circle marks the location where flux emerges at 04:00 UT. This image is from 2011 February 27, 13:00:07 UT.

The jet we observe has properties similar to features identified previously as macrospicules. According to the work of Bohlin et al. (1975), Dere et al. (1989), and others, macrospicules have lengths of ∼4000–40,000 km, widths of ∼4000–11,000 km, and lifetimes of a few to ∼40 minutes. Some seem to be restricted to cooler ($\lesssim 3 \times 10^5$ K) temperatures (Bohlin et al. 1975), although others have been observed at higher (∼1 MK) temperatures (Pike & Harrison 1997). The size, shape, and temperature range of our jet are typical of macrospicules. Our jet occurs in the non-active-region Sun (differentiating it from "surges"); it has no strong signature in AIA filters (e.g., 94 Å) which detect the hottest EUV plasmas, and so it likely is not an X-ray jet. Further, although we searched for the jet in *STEREO* (behind and ahead) in the 304 Å waveband, it was not visible, either because the event was too small or it was over the limb. *Hinode* had no observations for our event. However, the AIA and HMI data are ample for us to examine the eruption onset mechanism for this macrospicule jet.

2. INSTRUMENTATION AND DATA

Launched on 2010 February 11, the instruments from *SDO* have been providing simultaneous, multiple wavelength observations of the solar atmosphere. AIA has 0.″6 pixels, and a cadence of 12 s (sometimes faster for special observations). For more details on AIA, see Lemen et al. (2012). HMI is a 14 cm imaging instrument, tuned to the Zeeman-sensitive line at 6173 Å. The specifications of HMI include a precision of 10 G, dynamic range of ±4 kG, zero-point accuracy of 0.05 G, and spatial resolution of 1″ (0.″5 pixels). For more details on HMI, see Scherrer et al. (2012). The AIA data used in this study are primarily 171 Å, 193 Å, and 304 Å images with 12 s cadence and HMI magnetograms at 45 s cadence. All data were calibrated with standard Solarsoft routines.

For our study, we located a jet in a low-latitude coronal hole, close to disk center (see the box of Figure 1). Figure 2 zooms in on the regions of interest. The jet we are to examine occurred on 2011 February 27, in the rectangular-boxed region of Figures 1 and 2. An emerging flux episode occurred in the circled region of Figures 1 and 2, beginning at ∼ 03:25 UT; this did not produce a jet, but we will contrast it with the jet-producing region in Section 3.2. To determine the relationship between the jet and the magnetic field, we first visually aligned an *SDO*/AIA 193 Å image at 13:00:07 UT with a *SDO*/HMI line-of-sight magnetogram at 13:00:28 UT. We checked this alignment by overlaying sunspots visible on the solar disk in AIA 4500 Å images with the HMI magnetograms. For a final adjustment, we compared features in AIA 1600 Å images with the magnetograms in the immediate vicinity of the location of the jet event. As a result, we are confident that

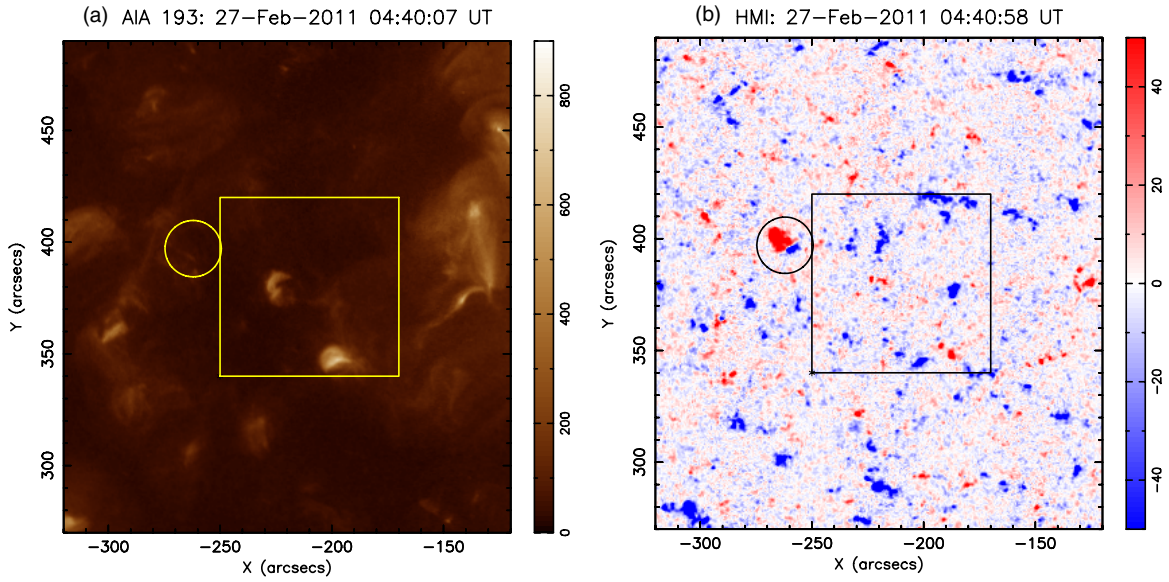

Figure 2. AIA 193 Å image (left) and a HMI magnetogram (right), showing regions of interest. Both images are from 2011 February 27, with the AIA image from 04:40:07 UT and the HMI image from 04:40:58 UT; red and blue represent positive and negative fluxes, respectively. The rectangle and circle show, respectively, regions where the macrospicule-like jet later occurs (13:00 UT) and a region where a new emerging flux region (EFR) occurs around 04:00 UT, but from which no jet is seen. The rectangle marks the same field-of-view as in Figures 3, 4, 9, and 11. North is upward and west to the right in these and all other images in this paper.

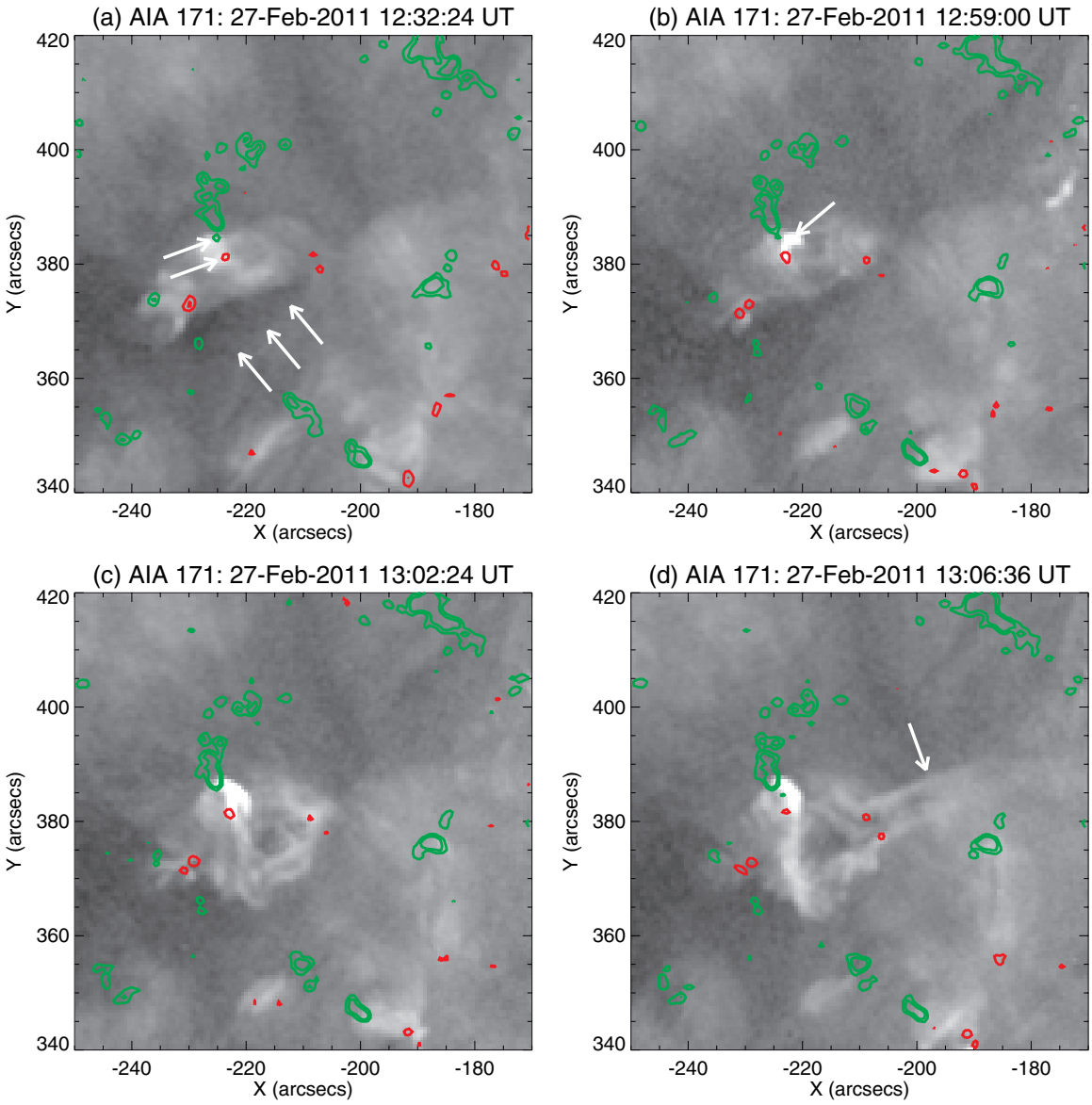

Figure 3. Images showing different phases of the jet evolution from the AIA 171 Å channel. Overlaid are line-of-sight magnetograms from HMI, with red and green respectively representing positive and negative polarities, with contours of 40 and 100 G. Times above the panels are for the AIA images, and the magnetograms are from about the same times, at 12:32:43 UT, 12:58:58 UT, 13:01:13 UT, and 13:06:28 UT, for panels (a)–(d), respectively. In (a), the two northern arrows indicate regions of enhanced magnetic flux, where the positive and negative polarities appear to be approximate footpoints of a bright arch between them. The three southern arrows outline the southern edge of a dark channel region, indicative of open field lines not viewed in projection against any perceptible emitting plasma in closed field low in the coronal hole. Panel (b) shows a brightening (arrow) at the start of the jet event. Panel (c) shows brightening spreading into the dark channel region, and panel (d) shows the jet (arrow). All of these solar images, and those of subsequent figures, have been derotated to a common time: 2011 February 27 12:30 UT.

(An animation of this figure is available in the online journal.)

our alignment between AIA and HMI is accurate to better than a few arcseconds.

With the alignment confirmed, we made movies at several AIA wavelengths of a $110'' \times 100''$ region centered on the jet. We then made HMI magnetogram movies of the same region. These videos formed the main data sets we initially examined.

3. OBSERVATIONS

3.1. Morphology and Evolution of the Jet

Figure 3 shows the evolution of the jet in AIA 171 Å images, and superimposed we show magnetogram contours from HMI. In this case we show only relatively strong fields of the region, with contours of 40 and 100 G. Figure 3(a) shows the situation prior to jet onset. The two northernmost arrows in this panel show locations of moderately strong field (that we measure to be ∼50 G) that anchor a brightening between them. From the movie corresponding to this figure, this brightening appears to be one arch in a more extensive arcade of field, with the axis of the arcade roughly oriented in the east–west direction. The east side of this arcade is approximately anchored by relatively moderately strong negative and positive polarities of magnitude ∼100 G each, located respectively at approximately $(-235'', 373'')$ and $(-228'', 372'')$ in this figure. The westernmost side of this arcade is partially anchored by the moderately strong positive flux elements near $(-210'', 380'')$. Negative-polarity anchoring fluxes for the arcade's west end are weaker and so not visible in this panel, but they are visible in Figure 5, discussed

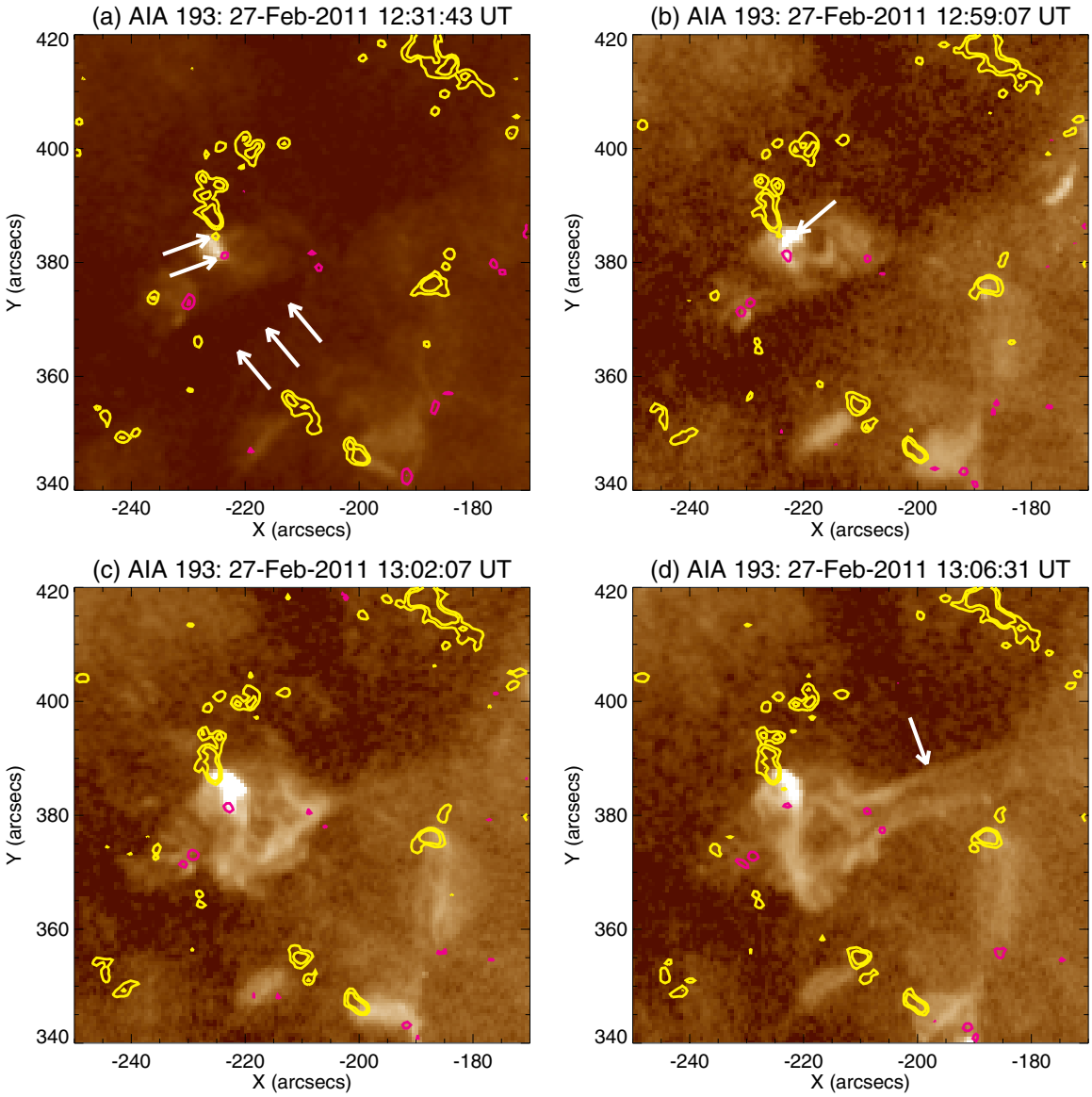

Figure 4. Same as Figure 3, except with images from the AIA 193 Å channel. Again the contours are for fields of 40 and 100 G, but yellow contours represent the negative polarity and magenta contours represent positive polarity. Times above the panels are for the AIA images, and the magnetograms are from about the same times, at 12:32:43 UT, 12:58:58 UT, 13:02:43 UT, and 13:04:58 UT, for panels (a)–(d), respectively.

below. At various times in the video accompanying Figure 3, this arcade shows brightenings, especially in the comparatively strong field locations. The south edge of this arcade traces out the north edge of a dark channel, and the three southernmost arrows of the panel approximately indicate the southern edge of the dark channel. This channel is dark because 171 Å coronal emission from plasma in low-lying magnetic loops is less there than in surrounding areas, perhaps because the closed field is weaker in the dark channel. Perhaps there is no perceptible coronal-temperature plasma in low loops along the line-of-sight in this channel, so that the 171 Å coronal emission in this channel comes only from the low-density, coronal-temperature plasma in the coronal hole's open field along this line-of-sight.

Figure 3(b) shows a localized region along the arcade that brightened, having the appearance of a loop structure. This brightening is the first stage of the impending jet, as seen in the 171 Å images. By the time of Figure 3(c), the brightening has extended over most of the region of the dark channel pointed out in Figure 3(a). Figure 3(d) shows a jet erupting from a location near the west end of the arcade feature, and the moderately strong positive polarities located there. As the jet fades, from about 13:10 UT, the 171 Å coronal images become similar to that of Figure 3(a) again, but the coronal dark channel becomes very dark in the 171 Å images, lasting until about 13:30 UT (see video accompanying Figure 3).

Figure 4 is the same as Figure 3, but for the 193 Å passband, which on average observes higher temperature coronal plasmas than the 171 Å filter; contribution functions for these filters peak at $\log T$ values of 6.2 and 5.8 K, respectively (Lemen et al. 2012). The larger $\log T$ results in a stronger contrast for the hot elements inside the coronal hole in the 193 Å images. The arrows of Figure 4 are the same as in Figure 3 for ease of comparison.

Figure 5 and the accompanying video show the same eruption in AIA 304 Å images. The field of view is smaller here than in Figure 3, to focus on the pre-jet eruption location. We also show weaker magnetic fields here, including contours of 10, 15, and 20 G, in addition to the 40 and 100 G used in Figure 2; by matching the 40 and 100 G contours it is possible to make

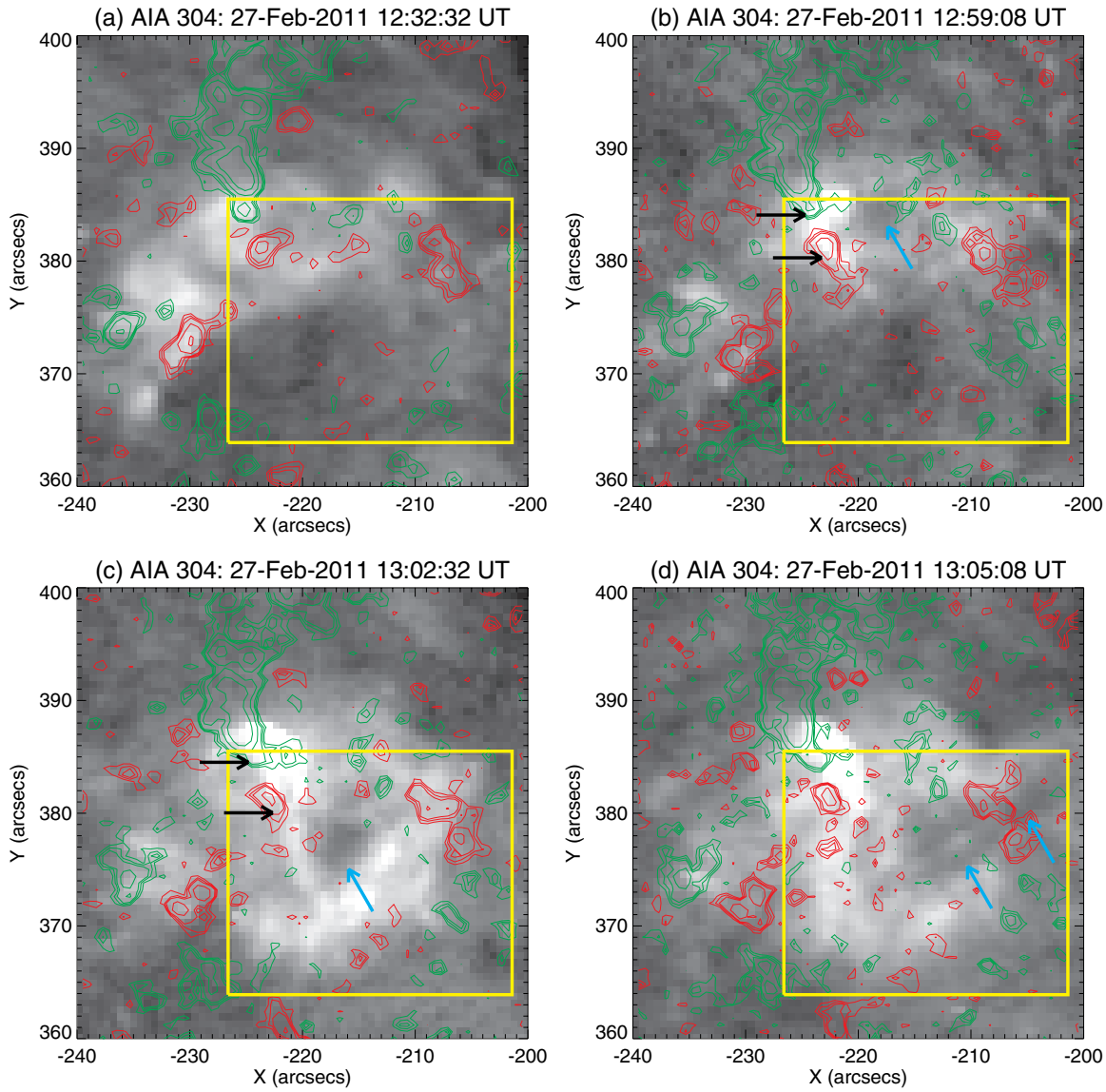

Figure 5. Same as Figure 3, except with images from the AIA 304 Å channel. In this case the contours are for fields of 10, 15, 20, 40, and 100 G. Times above the panels are for the AIA images, and the magnetograms are from about the same times, at 12:32:43 UT, 12:58:58 UT, 13:02:43 UT, and 13:04:58 UT, for panels (a)–(d), respectively. The black arrows in (b) and (c) indicate relatively strong magnetic field locations forming the bipolar footpoint of a bright loop that flares during the time the jet forms. Blue arrows in (b) and (c) point to an absorption feature, possibly a very small erupting filament, that initially shows motion to the south and then evolves into the jet. The yellow boxes show the area over which the flux in Figure 7 is determined.

(An animation of this figure is available in the online journal.)

connections with the Figure 3 images. We have also set the intensity scaling so that some features are saturated, in order to highlight some of the fainter features.

Since one model for jet onset is emerging flux interacting with an open field (Yokoyama & Shibata 1995, 1996), we can first look for evidence that the bright loop prominent in the pre-jet times of Figures 3(b), 4(b), and 5(b) is the bright feature that accompanies the emerging flux in those models (with that bright feature resulting from reconnection between the emerging closed field and ambient open field in the model). Yokoyama & Shibata (1996) call this feature a "hot loop" in their Figure 9, and Moore et al. (2010) call the same feature a "bright point." Adopting the "bright point" terminology here also, if the bright loop of Figure 3 corresponds to a bright point, then the flux emergence of the models should occur in the region between that bright loop and the southwest side of the jet. Such emerging flux would be expected in the yellow box region of Figure 5. No such new flux is obvious via visual inspection in the moderately strong fields of Figure 5, that is, at the 40 and 100 G levels. We will examine this question more closely in the next section.

In the 304 Å images much of the jet is a dark feature, prominent in Figure 5(d). By running these 304 Å images backward in time, we find that the material that forms this dark jet is a dark "blob" of size ∼3″–5″, that smoothly evolves into dark strands of the jet. This dark blob is prominent from about 12:58 UT, and we can trace the motions of either the same feature or precursor motions of fainter features back to at least 12:53 UT in the 304 Å video (these pre-12:58 UT features are very faint, and may have been separate from the post-12:58 UT feature that made the jet). After 12:58 UT, the pre-jet dark blob, indicated by blue arrows in Figures 5(b) and (c), moves ∼6″ southward (there could have been substantial movement outward from the Sun as well) over 12:58:00–13:02:32 UT, or

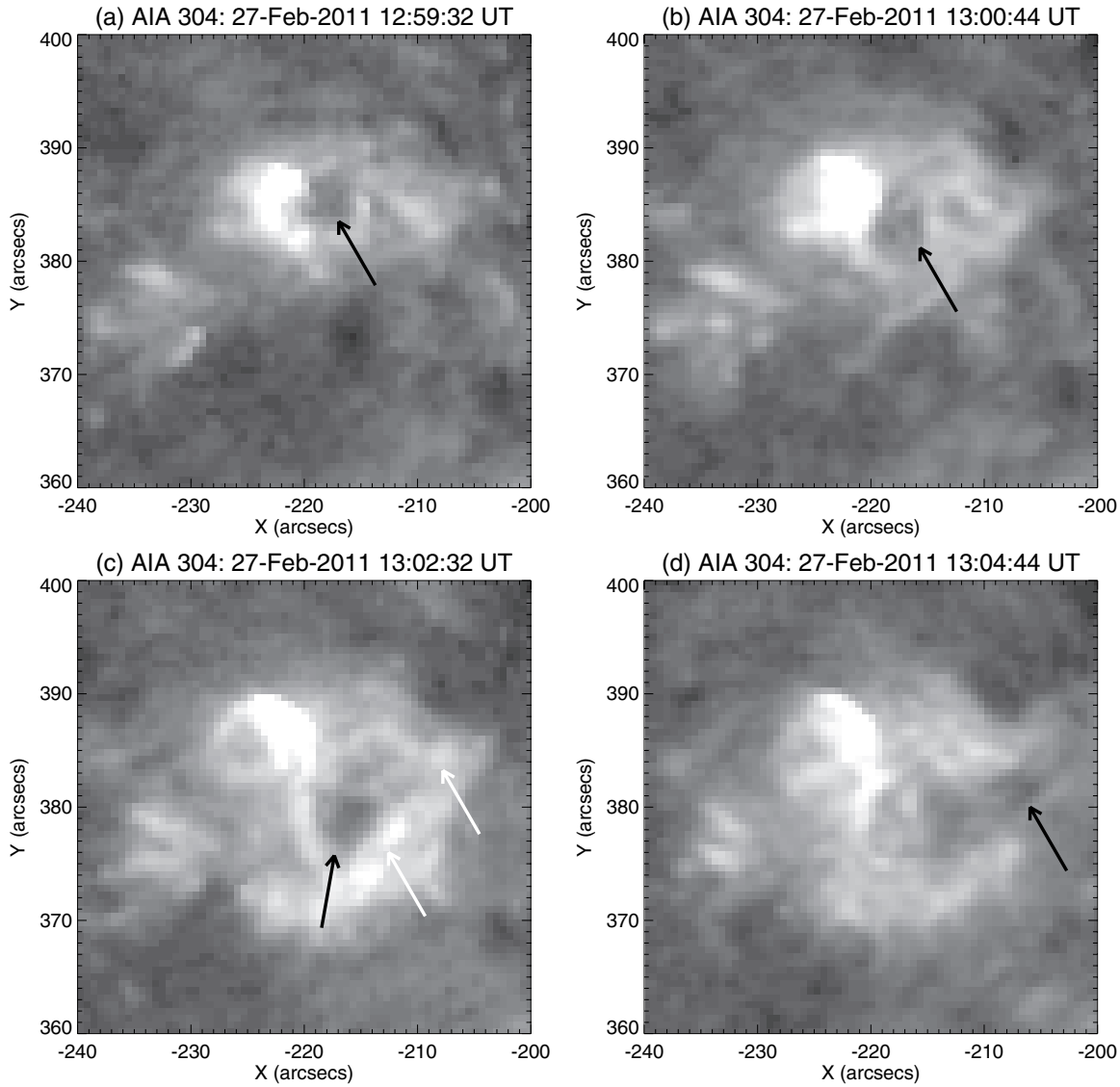

Figure 6. AIA 304 Å images of the erupting region, showing the onset of the dark "blob" motion in panels (a)–(c), with that blob transforming into the jet in (d). Although it is hard to be certain of the nature of the blob due to its small size, its evolution is similar to that of larger-scale solar filaments that erupt, sometimes ejecting larger-scale jets or a surge. Similar to some larger-scale erupting filaments, it is dark in 304 Å images prior to eruption, but develops brightenings in and/or around the dark material; the white arrows of (c) show such possibly similar brightenings around the erupting dark blob just prior to jet formation. The black arrows track the dark feature. In panel (d), the dark feature has become part of the out-flowing jet and covers an area that is bright before in panels (a)–(c), evidence that the dark feature is absorbing cool plasma, not a void.

(An animation of this figure is available in the online journal.)

$\sim$15 km s^{-1}, before losing its roughly circular appearance and showing an obvious primarily vertical movement. This change in direction, consistent with a turn onto vertical open field lines, occurs over the period 13:02:08–13:03:56 UT, and then from the frame at 13:04:32 UT (see video), the feature takes on an extended, jet-like structure. This blob appears to be a filament-like structure that elongates into a jet along the open field, similar to the behavior of surges in active regions; we will discuss this further in Section 4. Between 13:02:00 UT and 13:06:24 UT, during the jet's most rapid-movement phase, in the 171 Å and 304 Å images we measure velocities of 80 $\pm$ 11 km s^{-1}; this is in the plane of the image, and so the true velocity may be even $\sim$2 times faster. In the 193 Å images there is a faint, faster component that has a speed of $\gtrsim$200 km s^{-1}, over 13:02:31 UT and 13:03:07 UT. Figure 6 shows the blob in more detail, and will be discussed further in Section 4.

The jet brightens at its base for $\sim$2 minutes from $\sim$12:58 UT, and then from $\sim$13:02 UT it expands outward as a jet, extending to 20,000–40,000 km in 304 Å and 171 Å images, and somewhat larger ($\gtrsim$50,000 km) in 193 Å images; its lifetime is also filter-dependent. In 171 Å and 193 Å images it lasts for 10–12 minutes. In 304 Å images it is in emission also for about 10 minutes, but continues to be visible as an absorption feature for $\sim$10 minutes longer, for a total lifetime of $\sim$20 minutes. In all wavelengths it appears to fade, or diffuse and disperse, without much of the jet material showing falling motions. These properties match well with those reported for macrospicules.

3.2. Magnetic Changes

A question we consider is whether the proposed X-ray jet mechanisms discussed in Section 1 produce the cool jet

we observe here. Although our macrospicule-like jet contains relatively cool material, it is a coronal jet (with a chromospheric component), as we observe it in coronal lines. So we can examine whether the mechanism proposed for X-ray jets can also apply to this particular event. To this end, we examined the magnetic field changes of the jet region. Visually inspecting both the magnetograms themselves, and various contour levels of the magnetograms (Figures 3 and 4), we can detect no obvious bipoles emerging in the region including the jet and adjacent to the bright loop. Emerging bipoles would be required if the blowout X-ray jet mechanism suggested by Moore et al. (2010) produced the macrospicule with the observed bright loop corresponding to the jet's bright point, which would be made by external reconnection in the blowout scenario. (A discussion of external/internal reconnection may be found in Section 4.) The same basic initial magnetic field setup would be expected for the standard jet mechanism suggested by Shibata et al. (1992).

To examine in more detail possible flux emergence in the area where the expected bipole causing the jet should have emerged, we investigated the magnetic flux of the region bounded by the yellow box of Figure 5. This box is situated so that it abuts the bright loop in the northeast, which again is a candidate to be the possible Moore et al. (2010) "bright point" of the jet, and the box extends down to a location containing the entirety of the base of the macrospicule jet. The detailed placement for this box was selected, in part, so that it largely isolates patches of positive polarity within its boundaries for the duration of our measurement, so that there will be a relatively small amount of flux flow across the boundary with time; this is desired since such boundary flows could result in spurious measurements of the localized flux evolution (Green et al. 2003; Sterling et al. 2010a). Our selected box only isolates the positive flux, however, as the negative flux is not well-isolated in this box region. Hence we only consider the positive-flux variation, and plot the results in Figure 7 for the magnetic flux, $\int Bda$, where B is the magnetic field strength and da the area element, where B is normal to da and where the integral is over all of the positive flux in the box. We find the background level of the positive flux in this box to be $\sim 1.1 \times 10^{19}$ Mx. The total (peak-to-peak) variation of the flux in this box relative to the time-averaged flux over time of Figure 7 is within ~20%. There could be a slight increasing trend from about between 12:15 UT and 12:30 UT, where the flux is $\sim 11.1 \times 10^{19}$ Mx, and 13:10 UT and 13:30 UT, where the flux is $\sim 12.1 \times 10^{19}$ Mx; this is a ~9% increase over the ~1 hr time period, with an emergence rate of $\sim 3 \times 10^{15}$ Mx s^{-1}. Whether this is due to emergence of flux over this region cannot be determined from our examination of the data, and from the plot this variation is similar to the amplitude of the fluctuations with time over our measurement box. Another possibility is that it is due to residual flows of positive flux through the box boundary. Either way, we are able to say that if there is flux emergence over this region, it is of the magnitude of $\lesssim$10% of the boxed region's average (background level) flux for the two hour time interval of Figure 7.

We have also looked at the flux variation of the entire field of view of the Figure 5 panels, which encompasses essentially all of the region where flux emergence could have conceivably directly generated the macrospicule. Again the positive flux values are likely the most reliable over this region, as there is relatively strong negative flux that crosses the northern boundary and that may flow back and forth across that boundary with time. Even with this however, we find that positive, negative, and total net fluxes are all constant to less than 20% over the duration covered

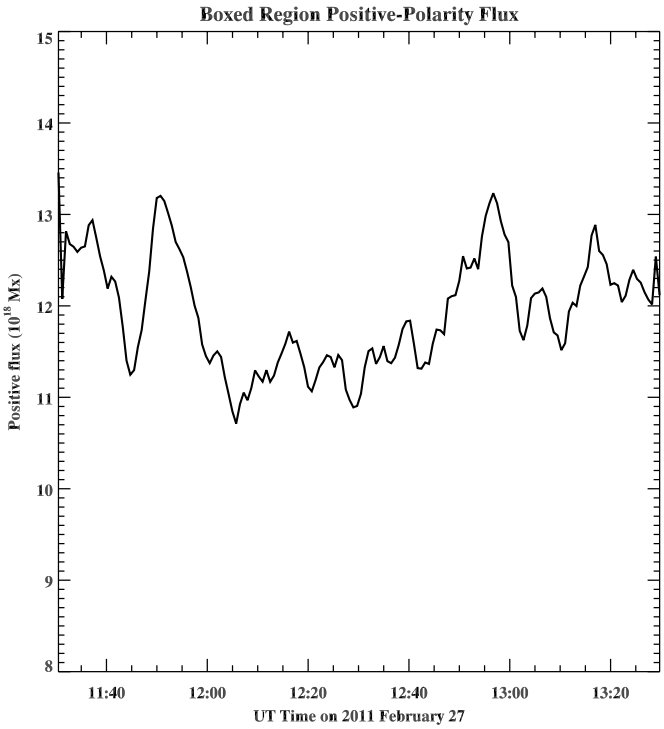

Figure 7. Positive-polarity magnetic flux as a function of time for the jet region, measured over the area of the yellow box of Figure 5. Only positive-polarity flux was measured, since only very little positive flux crosses the box boundary over the duration of the measurement, while the negative-polarity flux is not so readily isolated.

in Figure 5. This reaffirms that there is little flux emergence in this region over the time period around when the macrospicule jet is generated.

We contrast the magnetic situation of the jet with that of the emerging flux region (EFR) that occurred in the circled area of Figure 2. That flux emergence is unrelated to our jet event, and indeed has no jet accompanying it at all. It is however, an example of an obvious flux emergence occurring in the coronal hole; looking at its flux evolution can give us an idea of what might be expected if flux emergence of a similar size had occurred in the region of the macrospicule. Figure 8 shows the flux of the EFR region, where the size of the area integrated over in the integral of positive flux, $\int Bda$, is the same as that used above for the flux in the region of the macrospicule, i.e., the size of the yellow box in Figure 5; we do this so that we can directly compare the background fluxes of the EFR and the jet boxed regions. Initially, the positive flux in the EFR region is $\sim 1.4 \times 10^{19}$ Mx, which is very close to the average flux of the macrospicule region, showing that the background fluxes in the two regions are very similar. Starting at about 3:25 UT in Figure 8, from the steady background level, there is a jump in the positive flux value by about a factor of four, most of it occurring in ~20 minutes following 03:35 UT. The measured flux in the emerged EFR is well within the range of $(0.7–33) \times 10^{19}$ Mx for values found for EFRs in the neighborhood of quiescent filaments by Chae et al. (2001); their average value was 2.8×10^{19} Mx, which is about a factor of two smaller than what we find for our emerged EFR. Harvey (1993) found similar results for flux values of EFRs in quiet Sun, with a range of $(0.2–33) \times 10^{19}$ Mx, while Schrijver et al. (1998) found an average of 1.3×10^{19} Mx distributed over a range of $(0.3–3) \times 10^{19}$ Mx. The Chae et al. (2001) paper

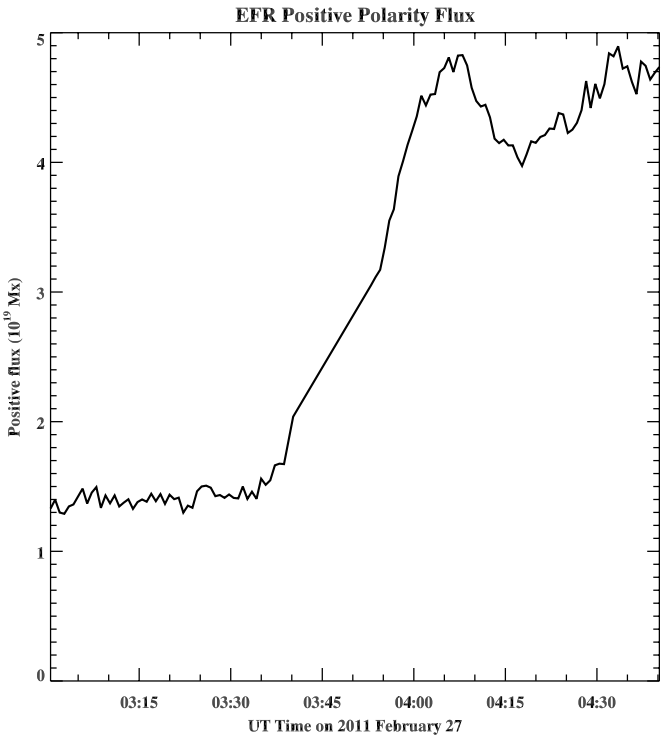

Figure 8. Positive-polarity magnetic flux as a function of time for the EFR of the circle of Figure 2. A box of the same size as that in Figure 5 and for the flux of Figure 6, was used for determining this EFR flux. As with the jet case, only the positive flux variation is shown here.

summarizes other EFR results in their Table 2, none of which are substantially different from those quoted here. Therefore, the feature we know unambiguously to be an EFR shows a substantial increase in flux by about a factor of four, while in contrast the flux changes in our macrospicule jet region around the time of the jet are ∼20%. So if emerging flux was the cause of the jet, then it was emergence of this relatively low amount.

We have been considering that the postulated bipole that would produce the macrospicule as a jet would be emerging, as part of an emerging flux system; this was explicitly considered in simulations of non-blowout jets, such as those of Yokoyama & Shibata (1995, 1996) and in the blowout-jet scenario mapped out in Moore et al. (2010). We can also consider whether the jet-base bipole had already completed most of its emergence, and thus was an emerged bipole that was disrupted somehow, reconnected with the open field, and subsequently underwent its own eruption. In order to investigate this possibility, we examined the location of the macrospicule jet with respect to the underlying magnetic flux, to see whether the jet sits on such a bipolar region. We show this in Figure 9, where, in order to increase the signal of the magnetic field, we integrated 160 HMI images over time spanning 11:30:29 UT to 13:29:44 UT and boxcar averaged the resulting image using a smoothing width of 8 pixels. Figure 9(a) shows the arcade containing the bright loop, which again would be the bright point that would brighten when the closed bipole field reconnects with the open field according to the X-ray jet models. Figure 9(b) is from the time of the jet and shows that the north side of the jet is located near the contoured positive field (black arrows) that is around 10 G. A negative field south of the jet is indicated by the white arrow in Figure 9(b). But that field does not fully reach the jet region, and moreover it is very weak; the contour of the white arrow is at the 2 G level. Even considering the alignment uncertainties of a few arcseconds determined in Section 2, there is no obvious negative flux to counter-balance the positive flux that would be part of an emerged bipole of substantial strength that could have blown out to make the jet. We can again confirm this alignment in Figure 9, by observing that the two ends of the bright loop north of the jet match well with the poles of a small-scale moderately strong bipole that form the loop's footpoints (cf. Figure 5(b)). Therefore, there is no evidence for an already emerged, substantially strong bipole to the south side of that bright-loop bipole and under the jet, as would be expected in the X-ray jet models if the brightest loop in this jet were the reconnection bright point, made by external reconnection of the closed field of the jet-base bipole when it impacted open field.

We conclude that neither an emerging or already emerged bipole south of the bright loop is likely to have been the cause of the macrospicule eruption, unless that process was at or below the emergence rate or flux levels indicated by our above analysis. Therefore we explore another possible jet-eruption-onset mechanism.

4. POSSIBLE MECHANISM

We have found that an eruption of a jet-like feature occurred in quiet Sun, without a recently emerged or concurrently emerging strong bipole underlying the jet. Thus it is not likely that an emerging or emerged bipolar flux region of size scale similar to that of the jet is the direct cause of this blowout macrospicule jet. We consider instead that the dark feature of Figures 3(c) and 4(c) that becomes the jet in Figure 3(d) is an erupting small-scale filament, similar to the large-scale filaments in arcade-blowout eruptions that produce a coronal mass ejection (CME) in tandem with a flare. As in large-scale filament eruptions, this small-scale filament eruption would begin with initial movement (slow-rise phase) that is not accompanied by strong flare-like brightenings (Roy & Tang 1975; Sakurai 1976; Martin 1980; Tandberg-Hanssen et al. 1980; Kahler et al. 1988; Sterling et al. 2010a; Règnier et al. 2011). The small-scale filament eruption could have started out similarly here, and then became the jet upon encountering the open magnetic field. Based on our observations, we can speculate as follows on how the eruption of this jet proceeded.

Figure 10 shows a schematic of the progression we propose for this eruption, overlaid onto the AIA 304 Å images of Figure 5, using the smoothed, averaged magnetogram of Figure 9. As shown in Figure 10(a), prior to the start of the eruption, the bright arcade is embedded in negative-polarity open field since this is a coronal hole having predominantly negative-polarity flux.

Figure 10 depicts that some unspecified mechanism makes the filament-like dark material start erupting; the dark material is carried inside an erupting loop of magnetic field. The outside of this erupting loop is represented by the solid dark blue lines in Figures 10(b)–(d). The initial horizontal motion is due to the flaring out of open field from the relatively strong patch of negative flux north of the eruption. The thicker black line in each panel represents the open guide field. Figure 10(c) shows the expelled filament-like feature and the closed field carrying it impacting the vertical open field. That is, the outside envelope (solid blue line) of the erupting loop field undergoes reconnection with the black open field lines. In addition to this external reconnection, internal reconnection between the outstretching legs of the dark blue field makes the compact bright arch that has started between the feet of the erupting blue

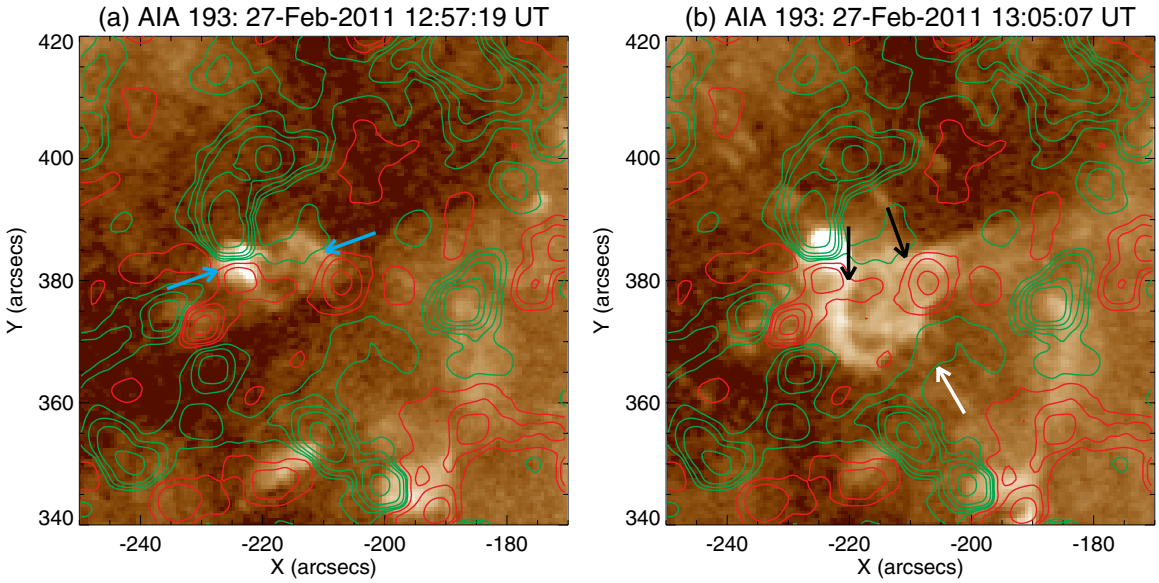

Figure 9. Images from the AIA 193 Å channel. Panel (a) is at a time before the jet forms and shows the pre-eruption arcade (blue arrows) that likely contains the minifilament, and panel (b), is at the time of the jet. Both images are overlaid with the same time-integrated and spatially averaged magnetogram as in Figure 12. In panel (b), the black and white arrows show locations of opposite-polarity flux that presumably forms a larger weak closed bipole south of the eruption. This bipole has a passive role in this jet.

loop in Figure 10(b). Here "external reconnection" refers to reconnection between the erupting magnetic loop and the open field outside that loop. In contrast, "internal reconnection" refers to reconnection between the legs of that erupting magnetic loop, and thus it is reconnection occurring inside of the erupting loop itself. See Figure 3 in Sterling & Moore (2001a) for a two-dimensional representation of these types of reconnection; that figure schematically depicts in two dimensions what Figure 10 here depicts in three dimensions. The external reconnection process between a closed loop and open field is also commonly referred to as "interchange reconnection" (see Crooker et al. 2002).

Figure 10(c) shows the dashed dark blue field line undergoing internal reconnection; this reconnection has resulted in the addition of a new dashed dark blue loop at the location of the strongest photospheric field, with the consequence of flare-like brightening of that and neighboring loops. Figure 10(c) also depicts the result of the external reconnection, shown by the turquoise field lines. One product of this external reconnection is closed loops (the turquoise loop) that are rooted in field not as strong as that making the relatively strong brightening of the loop of the dashed, dark blue field. The reconnection that produces the turquoise closed loops heats the plasma in those loops and the transition-region plasma in the feet of those loops, making the rim of emission seen especially prominently in Figure 10(c). The yellow patches in that panel represent footpoints of enhanced emission. Similar types of remote foot-point brightenings have also been seen during the onset of standard-scale solar eruptions (Sterling & Moore (2001a, 2001b), and Crooker et al. (2006) refer to such brightenings as "EIT crinkles"). Features consistent with transient loops that have these brightenings as footpoints are visible in the 304 Å images of Figures 10(c) and (d), and in other AIA wavelengths as well, perhaps best in 211 Å. The turquoise line of Figure 10(d) (oriented north/south) roughly traces one such possible loop. Also seen in Figure 10(c) and Figure 10(d) is the other product of the external reconnection, the turquoise open-field line. The erupting dark material is thus provided an escape path to flow outward into the corona, creating the jet. In this figure we only depict one pair of many such external reconnection field lines.

In this scenario, what leads to the initial disruption of the magnetic field containing the filament-like dark material is uncertain. But this is also frequently the case with standard-scale eruptions leading to flares and CMEs, when the filament starts to undergo its slow rise prior to rapid eruption. In studies of such events, one suggestion for the process that triggers the initial filament rise is flux cancellation. Innes & Teriaca (2013) have shown that cancellation can occur as the result of flows at the edges of supergranules; that is apparently occurring here. Between 00:00:24 UT (Figure 11(a)) and 02:14 UT (Figure 11(b), arrow), a clump of positive flux appears. From the movie of Figure 11, this flux clump apparently becomes enhanced by convergence of more-diffuse positive flux. The size and visibility of the flux clump waxes and wanes with time (Figures 11(c)–(e)), until much of this positive clump disappears into the negative flux to its north at about the time of the jet. By 15:06 UT, that positive flux has nearly completely disappeared (Figure 11(f)). This is the same positive flux indicated by the southernmost black arrow in Figures 5(b) and (c). Thus, this element is important in the magnetic configuration of the jet-producing region and it is likely that the cancellation of this element with nearby negative field was the trigger for the macrospicule jet.

We can trace back to early in its development the blob-like feature we suspect of being a minifilament that erupted and made the jet. We find that, as expected for filaments, this feature plausibly originates on a neutral line, albeit a very weak one; this is indicated by the 12:59:08 UT AIA 304 Å image of Figure 12(a), where the weak neutral line can be seen in the same time-integrated, boxcar-averaged HMI field used in Figure 9. In Figure 9(a) the feature appears to be centered about $\sim 3''$ away from the neutral line to its north; this offset from the neutral line may be due to the evolution of the fields over the two hours of the field integration, alignment uncertainty, or both. If this minifilament originates from that nearby neutral line, that would mean that it originated inside of the arcade roughly following

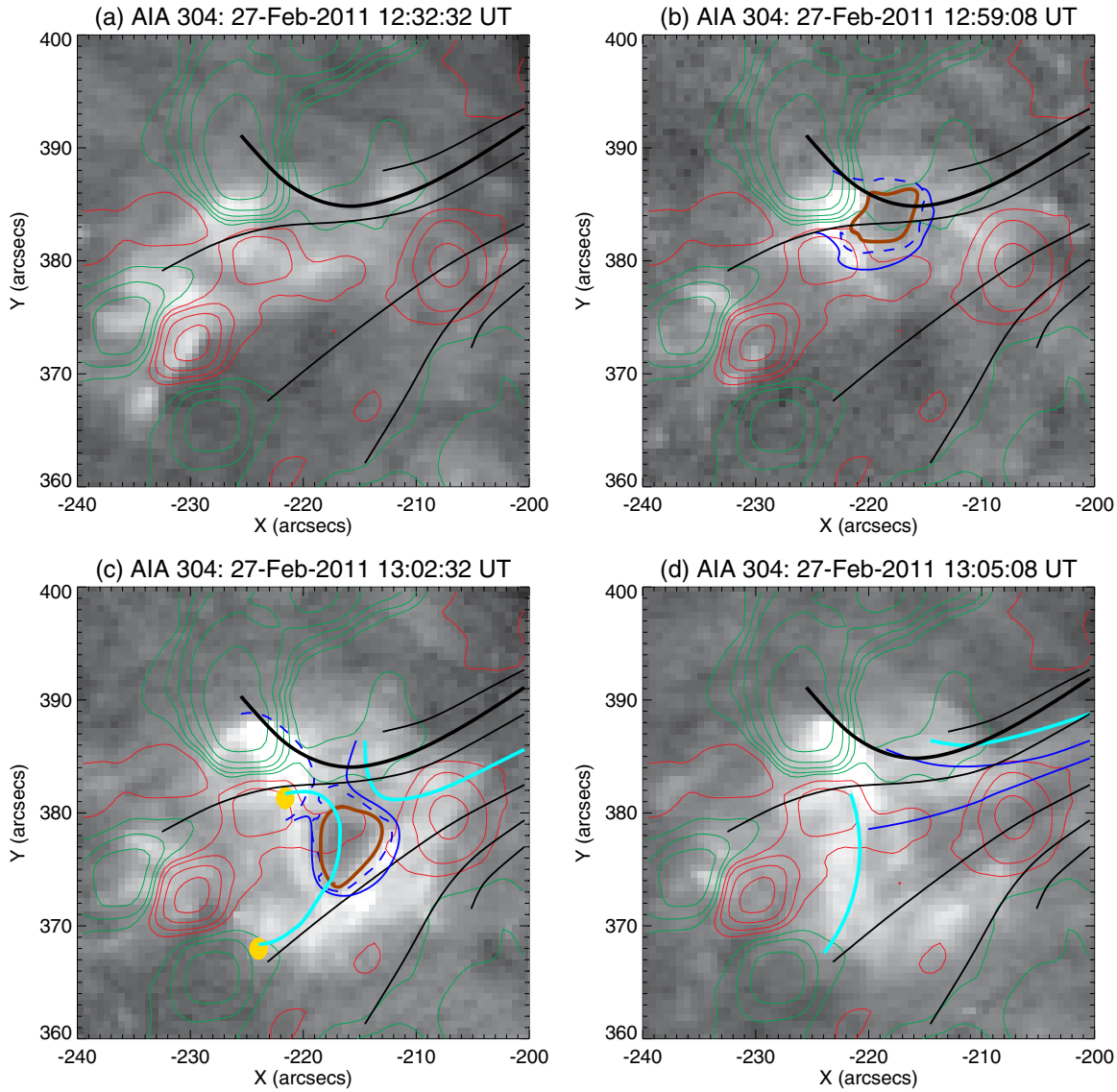

Figure 10. AIA 304 Å images of Figure 5 overlaid with the time-integrated spatially averaged magnetogram of Figure 9, with schematic lines added showing expected and postulated coronal magnetic field lines. Black lines in all panels show expected open field lines, along which the jet travels in (d); the open field is rooted in negative (green) polarity, with only a few field lines in the neighborhood of the jet displayed here. The thick dark-red closed circular-loop near the centers of the panels in (b) and (c) outlines the dark erupting minifilament material, which becomes part of the jet in (d) (with the enveloping dark-red lines omitted in (d) for clarity). Dark blue solid and dashed lines in (b)–(d) represent magnetic field lines enveloping the erupting minifilament material. The dashed dark blue lines in (b) are rooted in the strongest photospheric field of the region, and pinch off in (c) after they undergo internal reconnection, with the new dashed dark blue loop of (c) representing a loop of the flare-like brightening (dashed blue lines omitted in (d) for clarity). Turquoise lines of (c) and (d) depict field lines resulting from external magnetic reconnection between the dark blue field enveloping the erupting filament and the black open field lines. The footpoints of the newly reconnected field lines, especially that of the newly formed closed field, have enhanced brightening, indicated by the yellow patches, due to energy deposited in the closed-loop field by the magnetic reconnection. For simplicity, only one set of such reconnected field lines is depicted, but they would exist at many locations, making the bright circular fan of loops connecting the positive flux of the erupting arcade to negative flux at the southern feet of the jet.

that neutral line, visible in Figure 12(a) and pointed out by the blue arrows in Figure 9(a).

Another characteristic of "typical" filaments is that they are seen in absorption against the solar disk in chromospheric or sometimes coronal lines. Because of the blob-like feature's dark appearance against the disk, and because it originates near a neutral line, it is plausible that it could be a true filament on a miniature size scale prior to eruption. Although typical filaments are dark against the solar disk in 304 Å images, parts of them, or regions enveloping them, can turn into emission in 304 Å images during the eruption itself (e.g., Sterling et al. 2011). The dark blob shows such enveloping emissions in 304 Å starting between the time we can detect its motion and the time that the jet forms (Figure 6). Small-scale filaments have been observed to be the source of some jets, such as in the blowout jets of Shen et al. (2012) (see especially their Figure 2; also see Figure 5 of Moore et al. 2013, for examples of erupting filaments forming jets). We are hypothesizing that here we are seeing the same type of filament eruption as in those examples, except that the size scale of our miniature filament is about a factor of 10 smaller than those that Shen et al. (2012) and Moore et al. (2013) observed, which were $\approx 50''$ and $\approx 30''$, respectively.

Whether the pre-eruption blob-like feature we observe in Figures 3(c), 4(c) and 6 is truly absorbing material is difficult to determine due to its small size. Another possibility is that it is a combination of a void and bright loops that expand

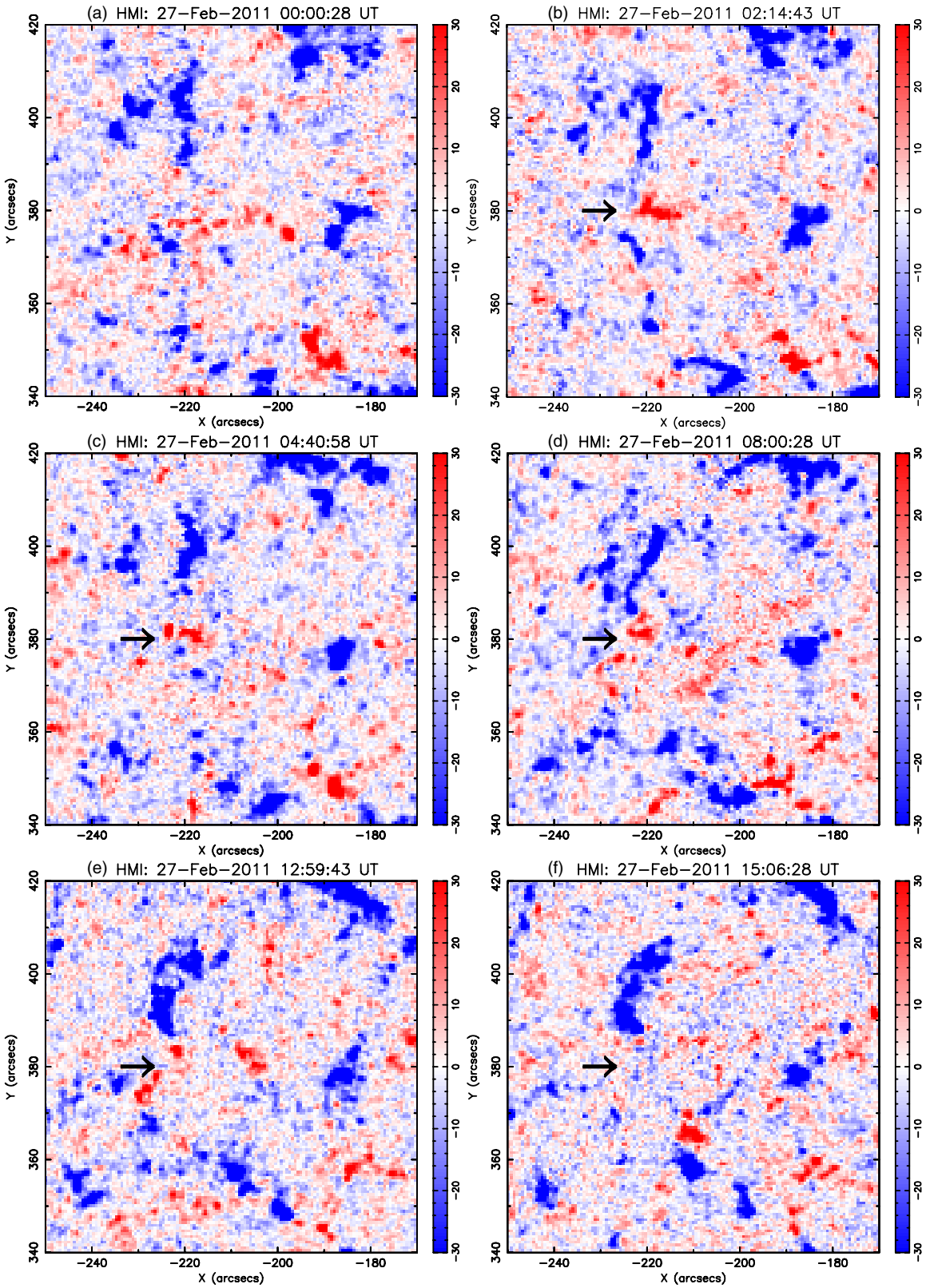

Figure 11. HMI magnetograms, as that of Figure 2(b), for the indicated times. These panels show the evolution of a positive magnetic flux element. The arrow serves as a fiducial, pointing to the location of the positive flux element in panel (b). This element may originally have been a network flux element at the time of panel (a). Eventually, the element cancels with negative flux to its north ((e) and (f)). This cancellation occurs near the location of and at about the time as the onset of the motion of the dark blob material that eventually erupted as the jet. The southernmost black arrow in Figure 5 points to this same positive flux element. A video of the evolution of the positive flux element and its merging with the negative flux to its north may be found in the online journal.

(An animation of this figure is available in the online journal.)

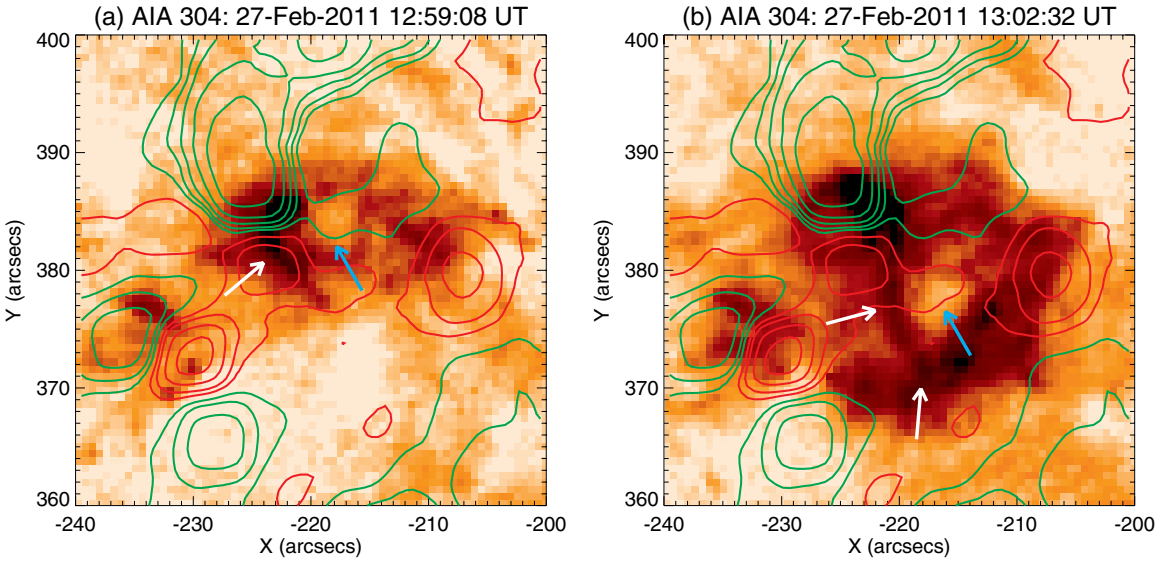

Figure 12. Negative images from the AIA 304 Å channel from (a) before the minifilament-like dark blob has moved substantially from the location where it was first detectable, and (b) as the dark blob is moving outward just prior to jet formation. Both images are overlaid with a magnetogram that is boxcar averaged with a constant smoothing window width of 8 pixels, of 160 HMI images over 11:30:29 UT to 13:29:44 UT on 2011 February 27. Contours are at ±2, 5, 10, 15, 20, and 40 G, and red and green contours respectively represent positive and negative fields. Blue arrows show the dark blob. The white arrow in (a) points to the bright loop, and the white arrows in (b) show arcade fields that are distended and brightened by the erupting field inside them that carries the dark blob. The southern white arrow in (b) points to a bright region magnetically connected back to the flaring bright loop.

outward, which then proceed to produce the jet. We believe however, that this feature is absorbing, since Figure 6 shows that it obscures brighter background material. Independent of whether it is a filament of absorbing material or a void plus bright-loop combination, the moving feature we observe prior to the jet likely marks the path of erupting magnetic field that forms the jet; that is, we expect the physical processes to be the same whether the dark blob is a miniature filament or a void and bright-loop feature. Either way, we will continue to refer to this pre-jet formation feature as a dark, blob-like feature.

As the field carrying the blob-like material inside this arcade erupts, it distends the legs of the enveloping field of the arcade, as shown in Figure 10. The strongest fields of this arcade are rooted in the bright loop indicated by the left blue arrow of Figure 9(a), and this bright arcade would be made larger and brighter by the reclosing-internal reconnection of the stretched legs of the envelope field as depicted by the dashed blue lines in Figure 10(c). This is the same as the internal reconnection resulting in flares according to the standard flare model, and also as in blowout jets as described by Moore et al. (2010). That is, the bright loop is a standard-type, solar-flare arcade accompanying the eruption of the minifilament that initially resides further to the west along the arcade above a neutral line. We conclude that the bright loop is *not* the "bright point" made by external reconnection of X-ray jet models; instead, it is made by the internal reconnection of the legs of the erupting arcade field.

5. DISCUSSION

We have found that the X-ray jet models based on emerging magnetic field do not apply to the macrospicule we observe here. Our observations do match the model proposed in Moore et al. (2010) for blowout jets in that the topology of the magnetic field in the base of our jet is the same as in that model. Even so, the relative size scales of the two sets of magnetic loops in the base of the jet are quite different. In the Moore et al. (2010) case, the external-reconnection-produced "bright-point" loops are relatively small and compact compared to the internal-reconnection-produced flare-arcade loops. What we have found for the macrospicule jet here is the opposite: the external-reconnection-produced magnetic loops are much larger than the internal-reconnection-produced loops. This reversal of the relative size of the two reconnection-produced sets of loops was not recognized as a possibility by Moore et al. (2010). Although the topologies of the Moore et al. (2010) schematic and our observed event are basically the same, the "bright-point" in the Moore et al. (2010) schematic is not the compact bright loop of our event. In addition, in our jet, the magnetic arcade that blew open was an evolved arcade; the possibility of the base arcade not being newly emerged was not recognized in Moore et al. (2010) either. In these two respects, our jet is a newly recognized variety of blowout jet. We cannot yet say how rare or common this variety may be for blowout macrospicule EUV jets and blowout X-ray jets.

Our observations indicate that the dark blob-like material that erupted in our jet was held in the field inside the arcade before it erupted, and was carried in this field in the blowout eruption of the arcade, as in the eruption of filaments in CME-producing blowout eruptions of much larger arcades. We have found that the blowout eruption in this case was likely the eventual outcome of flux cancellation from converging flows at the edge of a supergranule. Although we cannot totally rule out flux emergence as the trigger of the jet, any such emergence would have been at a level $\lesssim$20% that of the background magnetic flux in the region.

The blown-out material and its field encountered vertical open field, where external magnetic reconnection allowed the material to transfer to the open field. The other product of the external reconnection was newly formed magnetic loops with weak EUV brightenings at their footpoints. The strongest field lines attached to the outward-moving material were rooted in the strongest photospheric flux in the arcade, and some of these stretched field lines underwent internal reconnection under the erupting minifilament, producing flare loops in that portion of

the arcade that were noticeably smaller than the loops made by the external reconnection. The transferred blob material moved outward along the open field, forming the macrospicule jet. How often macrospicules or similar jets form in this fashion is a question to be addressed via examination of more events.

In the blowout jet observed by Shen et al. (2012), they proposed that external reconnection led to the rising of the filament as well as the jet. In their case, the mini-filament erupted adjacent to or even inside of the open field upon which it appeared as a jet, and therefore it is quite plausible that the external reconnection triggered the filament's eruption. In our case, however, the initial blob-like feature is displaced from the open field upon which the jet arises, and so it is equally plausible that the blob-like feature would have erupted even without the external reconnection with the open field.

We have been referring to the jet as a macrospicule that develops out of an erupting minifilament. Categorizing the type of jet, however, is not straightforward based on pre-*SDO* descriptions of macrospicules and minifilament eruptions by, e.g., Wang et al. (2000). Such descriptions must be reassessed in the *SDO* era.

A.C.S. and R.L.M. were supported by funding from NASA's Office of Space Science through the Living With a Star Targeted Research & Technology Program.

REFERENCES

Beckers, J. M. 1972, ARA&A, 10, 73
Blake, M. L., & Sturrock, P. A. 1985, ApJ, 290, 359
Bohlin, J. D., Vogel, S. N., Purcell, J. D., et al. 1975, ApJL, 197, L133
Chae, J., Martin, S. F., Yun, H. S., et al. 2001, ApJ, 548, 497
Cirtain, J. W., Golub, L., Lundquist, L., et al. 2007, Sci, 318, 1580
Crooker, N. U., Gosling, J. T., & Kahler, S. W. 2002, JGR, 107, 1028
Crooker, N. U., & Webb, D. F. 2006, JGR, 111, A08108
Dere, K. P., Bartoe, J. F., Brueckner, G. E., Cook, J. W., & Socker, D. G. 1989, SoPh, 119, 55
Green, L. M., Démoulin, P., Mandrini, C. H., & van Driel-Gesztelyi, L. 2003, SoPh, 215, 307
Harvey, K. L. 1993, PhD thesis, Utrecht Univ.
Huang, Z., Madjarska, M. S., Doyle, J. G., & Lamb, D. A. 2012, A&A, 548, A62
Innes, D. E., Genetelli, A., Attie, R., & Potts, H. E. 2009, A&A, 495, 319
Innes, D. E., & Teriaca, L. 2013, SoPh, 282, 453
Kamio, S., Curdt, W., Teriaca, L., Inhester, B., & Solanki, S. K. 2010, A&A, 510, L1
Kahler, S. W., Moore, R. L., Kane, S. R., & Zirin, H. 1988, ApJ, 328, 824
Labonte, B. J. 1979, SoPh, 61, 283
Lemen, J. R., Title, A. M., Akin, D. J., et al. 2012, SoPh, 275, 17
Martin, S. 1980, SoPh, 68, 217
Moore, R. L., Cirtain, J. W., Sterling, A. C., & Falconer, D. A. 2010, ApJ, 720, 757
Moore, R. L., Sterling, A. C., Falconer, D. A., & Robe, D. 2013, ApJ, 769, 134
Moore, R. L., Tang, F., Bohlin, J. D., & Golub, L. 1977, ApJ, 218, 286
Nisticò, G., Bothmer, B., Patsourakos, S., & Zimbardo, G. 2010, AnGeo, 28, 687
Pike, C. D., & Harrison, R. A. 1997, SoPh, 175, 457
Règnier, S., Walsh, R. W., & Alexander, C. E. 2011, A&A, 533, L1
Roy, J.-R. 1973, SoPh, 32, 139
Roy, J.-R., & Tang, F. 1975, SoPh, 42, 425
Sakurai, T. 1976, PASJ, 28, 177
Scherrer, P. H., Schou, J., Bush, R. I., et al. 2012, SoPh, 275, 207
Schrijver, C. J., Title, A. M., Harvey, K. L., et al. 1998, Natur, 394, 152
Shen, Y., Liu, Y., Su, J., & Deng, Y. 2012, ApJ, 745, 164
Shibata, K., Ishido, Y., Acton, L. W., et al. 1992, PASJ, 44, L173
Sterling, A. C. 2000, SoPh, 196, 79
Sterling, A. C., Chifor, C., Mason, H. E., Moore, R. L., & Young, P. R. 2010a, A&A, 521, A49
Sterling, A. C., Harra, L. K., & Moore, R. L. 2010b, ApJ, 722, 1644
Sterling, A. C., & Moore, R. L. 2001a, JGR, 106, 25227
Sterling, A. C., & Moore, R. L. 2001b, ApJ, 560, 1045
Sterling, A. C., Moore, R. L., & Freeland, S. L. 2011, ApJL, 731, L3
Tandberg-Hanssen, E., Martin, S. F., & Hansen, R. T. 1980, SoPh, 65, 357
Wang, J., Li, W., Denker, C., et al. 2000, ApJ, 530, 1071
Yokoyama, T., & Shibata, K. 1995, Natur, 375, 42
Yokoyama, T., & Shibata, K. 1996, PASJ, 48, 353
Zhang, J., Wang, J., Lee, C.-Y., & Wang, H. 2000, SoPh, 194, 59